# Adaptive Cutting Force Observer for Machine Tool Considering Stage Parameter Variation

Koh Ohno, Hiroshi Fujimoto
*The University of Tokyo*
5-1-5, Kashiwanoha, Kashiwa, Chiba, 277-8561, JAPAN
ohno.koh19@ae.k.u-tokyo.ac.jp, fujimoto@k.u-tokyo.ac.jp

Yoshihiro Isaoka, Yuki Terada
*DMG MORI CO., LTD.*
362, Idono, Yamatokoriyama, Nara, 639-1183 JAPAN
yo-isaoka@dmgmori.co.jp, yk-terada@dmgmori.co.jp

***Abstract*—Monitoring cutting force generated during the machining process is crucial to prevent tool breakage and chattering. The cutting force observer, which considers the machine tool as the two-inertia system, has been proposed to estimate cutting forces in wide bandwidth using multiple encoders. However, modeling errors and the parameter variation during machining can deteriorate estimation accuracy in such a model-based observer. Previous studies solved some modeling error issues, but inertia, friction, and other parameters that belong to the moving stage had rarely considered. Therefore, the adaptive cutting force observer is proposed in this paper. The proposal consists of online stage parameter identification and updating algorithm. The effectiveness of the proposed adaptive observer is demonstrated through the experiments using the simplified experimental setup.**

***Index Terms*—Machine tool, Cutting force observer, Adaptive observer, Two-inertia system.**

## I. Introduction

Automatic machinings using machine tools support today's industries. Among them, cutting is often used in a finishing process, and the accuracy of cutting has a significant influence on the precision and the quality of products. In other words, machining errors in the cutting process greatly affect the quality of the products. Chatter vibration, high load on the tool, and tool wear are well-known causes of machining errors. The cutting force is attracting attention as a useful parameter in the tool wear monitoring and the tool brakeage prevention [1]–[3]. Therefore, instead of using expensive sensors to detect the cutting force, sensorless force estimation using the motor information in a machine tool has been studied [4]–[6]. In recent years, a cutting force observer that uses a linear encoder to measure the position of the stage in addition to the motor's rotary encoder, has been proposed [7], and broadband force estimation without the effect of resonance has been achieved. However, the model-based force observers have the fundamental problem that estimation accuracy deteriorates when the plant parameters are changed [8]. It is a significant issue in machine tools where the mass of workpiece changes due to removal operations.

In order to deal with parameter fluctuations assuming cutting force estimation, robust estimation methods of torsional torque (the torque applied to the load-side, such as the moving stage) focusing on the motor and the transmission part such as the ball-screw, and methods focusing on the nonlinear rigidity of the ball-screw have been proposed [9], [10]. On the other hand, adaptive force observer is invented in [11]. Still, the two-inertia system is not taken into account. Anyway, it has not considered the mass of the load-side parameters, which varies steadily during and at every machining step. Therefore, in this study, we propose an adaptive identification of the cutting force observer that takes into account the variation of the stage parameters, and experiments confirmed its effectiveness.

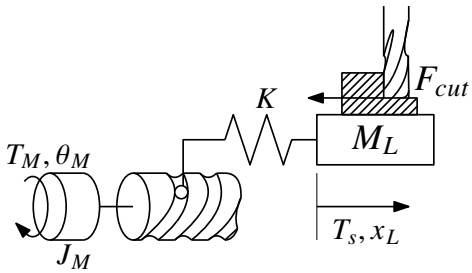


Fig. 1. Machine tool with ball-screw stage.

## II. Experimental setup

As a theoretical test of the machine tool, we don't use the machine tool itself, but an experimental setup with the same characteristics as the machine tool. First, it is known that the ball-screw stage used in a machine tool can be modeled as a two-inertia system. The two-inertia system consists of the motor-side inertia $J_M$, the stiffness of the transmission part $K$, and the mass of the motor-side $M_L$ as shown in the Fig. 1, and the cutting force observer proposed in previous study [7] also utilizes this feature. Therefore, the proposed method is verified by using an experimental setup shown in Fig. 2, which has the same characteristics as a machine tool as the two-inertia system. In this experimental machine, the motor-side and the load-side motor are connected with a shaft, which reproduces the two-inertia system's characteristics. $T_M$ is the motor-side motor's torque, and $T_s$ is the torsional torque transmitted to the load-side through the shaft, and $\omega_M$ and $\omega_L$ are the motor angular velocity on each side. The load-side motor can reproduce the input that simulates the cutting force, treated as $F_{cut}$. $F_{cut}$ is calculated from the drive current of the load-side motor.

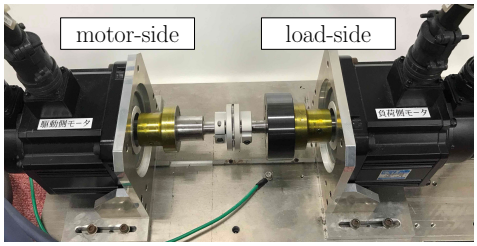


(a) Photograph.

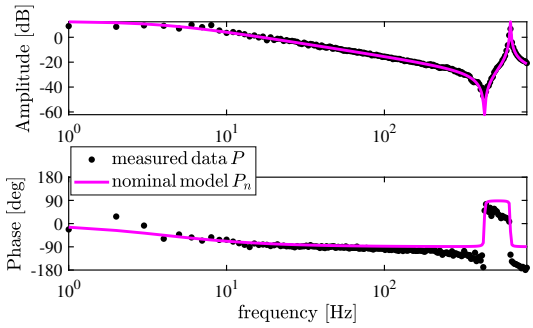


(b) Frequency response.

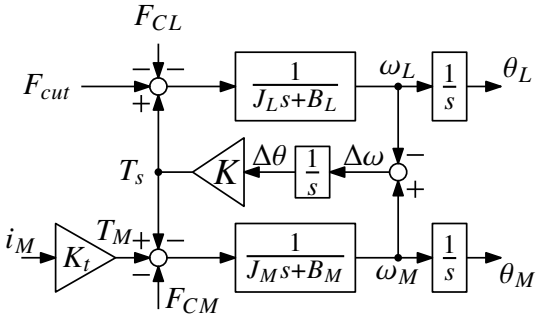


(c) Block diagram of two-inertia system model

Fig. 2. Experimental setup (The two-inertia system motor bench).

TABLE I
IDENTIFICATION RESULTS OF NOMINAL PARAMETERS.

| | | |
|---|---|---|
| Motor-side inertia | $J_M$ | $2.80 \times 10^{-4}\,\mathrm{kgm^2}$ |
| Motor torque constant | $K_t$ | $0.5710\,\mathrm{NmA^{-1}}$ |
| Torsion stiffness | $K$ | $1.7 \times 10^4\,\mathrm{N/mm^2}$ |
| Load-side inertia (w/o weight) | $J_L$ | $2.80 \times 10^{-4}\,\mathrm{kgm^2}$ |
| Motor-side viscus friction coefficient | $B_M$ | $0.002\,\mathrm{Nm/rad/s}$ |
| Load-side viscus friction coefficient | $B_L$ | $0.002\,\mathrm{Nm/rad/s}$ |
| Motor-side Coulomb friction | $F_{CM}$ | $0.15\,\mathrm{N\,m}$ |
| Load-side Coulomb friction | $F_{CL}$ | $0.15\,\mathrm{N\,m}$ |

Here, the nominal model $P_n(s)$ is defined as third-order transfer function which is modeled from the drive current $i_M$[A] to the angular velocity $\omega_M$ [rad/s] measured by the motor-side encoder (Fig. 2(b)). The nominal parameters shown in Table I were obtained by curve-fitting to the measured frequency response. Note that the motor-side Coulomb friction $F_{CM}$ and the load-side Coulomb friction $F_{CL}$ were measured separately.

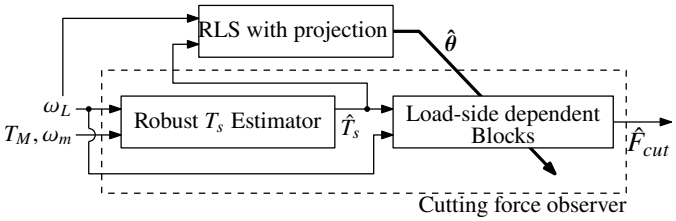


Fig. 3. Block diagram of the proposed adaptive cutting force observer.

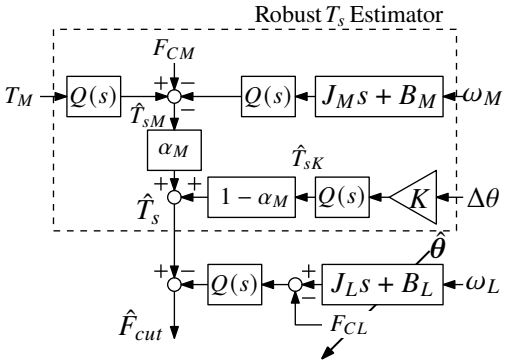


Fig. 4. Block diagram of cutting force observer based on robust torsion torque estimation [9].

## III. ADAPTIVE CUTTING FORCE OBSERVER

The structure of the proposed adaptive cutting force observer is shown in Fig. 3. The proposed observer consists of robust torsional torque estimation [9] and the algorithm to identify model parameters. The block indicated as RLS is the conditional parameter identification algorithm using recursive least square (RLS), which is added in the proposal. The cutting force observer is updated using the identified model parameters in the RLS block to make the observer adaptive.

The first and second part of this section describes the cutting force estimation scheme and robust torsional torque estimation, which are part of the proposed method. Then, the third part explains the parameter estimation algorithm and the adaptation idea focused on the load-side.

### A. Cutting force observer

The block diagram of the cutting force observer adopted in this paper is shown in Fig. 4. The blocks surrounded by dashed lines in the figure provides a robust estimation of torsional torque $T_s$. At the same time, the combination of $\omega_M$ and $\omega_L$ measurement performs broadband cutting force estimation [7].

The equation of motion about the load-side inertia $J_L$ is represented as below with the torsional torque $T_s$ as input.

$$T_s = J_L \cdot \dot{\omega}_L + B_L \cdot \omega_L + F_{CL} \cdot \mathrm{sgn}(\omega_L) + F_{cut}, \qquad (1)$$

$F_{CL}$ is a friction term that depends on the direction of velocity. When the torsional torque $T_s$ is estimated as $\hat{T}_s$ by the method

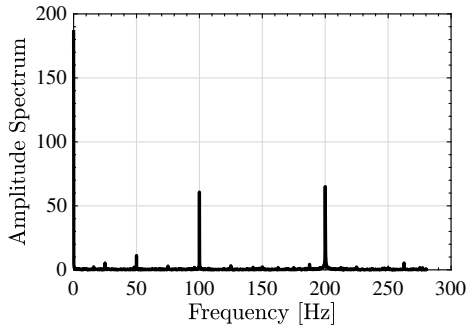


Fig. 5. Frequency analysis of the estimated cutting force in actual cutting with NVX5080.

described below, the following equation allow us to estimate the cutting force as $\hat{F}_{cut}$.

$$\begin{aligned}\hat{F}_{cut} &= Q(s)F_{cut} \\ &= \hat{T}_s - Q(s)\Big\{J_L s\omega_L + B_L\omega_L + F_{CL}\cdot\mathrm{sgn}(\omega_L)\Big\} \quad (2)\end{aligned}$$

Note that $Q(s)$ is a first-order low-pass filter (LPF), and $\hat{T}_s$ is estimated in the bandwidth of $Q(s)$.

### B. Robust torsional torque estimation

The robust torsional torque estimation, surrounded by dashed line in Fig. 4, is achieved by combining the two estimation methods described below and mixed with a mixture ratio $\alpha_M$.

$$\begin{aligned}&\hat{T}_{sM} \\ &= Q(s)\Big(T_M - J_M s\omega_M - B_M\omega_M - F_{CM}\cdot\mathrm{sgn}(\omega_M)\Big)\end{aligned} \quad (3)$$

$$\hat{T}_{sK} = Q(s)\frac{1}{s}(\omega_M - \omega_L)K = Q(s)\Delta\theta K \quad (4)$$

$\hat{T}_{sM}$ is the estimation by motor-side disturbance observer [12], and $\hat{T}_{sK}$ is the estimation method focusing on the relative displacement between the motor-side and load-side [13]. The estimation of torsional torque with minimum error variance for modeling and measurement errors is achieved by giving $\alpha_M$ as

$$\alpha_M = \frac{\sigma^2_{\hat{T}_{sK}}}{\sigma^2_{\hat{T}_{sM}} + \sigma^2_{\hat{T}_{sK}}}, \quad (5)$$

when the error variance of each estimation is represented by

$$\begin{aligned}&\sigma^2_{\hat{T}_{sM}} \\ &= \dot{\omega}^2_M\sigma^2_{J_M} + \omega^2_M\sigma^2_{B_M} + J^2_M\sigma^2_{\dot{\omega}_M} + B^2_M\sigma^2_{\omega_M} + \sigma^2_{F_{CM}}\end{aligned} \quad (6)$$

$$\sigma^2_{\hat{T}_{sK}} = (\theta_M - \theta_L)^2\sigma^2_K + K^2\sigma^2_{\theta_M} + K^2\sigma^2_{\theta_L}. \quad (7)$$

Where $\sigma_{J_M}$, $\sigma_{B_M}$, $\sigma_{F_{CM}}$ and $\sigma_K$ are modeling error variance of corresponding parameters, and $\sigma_{\omega_M}$, $\sigma_{\dot{\omega}_M}$, $\sigma_{\theta_M}$ and $\sigma_{\theta_L}$ are the measurement error variance. The measurement error variance due to encoder quantization noise is given by

$$\sigma^2(q) = \int_{-\frac{q}{2}}^{\frac{q}{2}} \frac{1}{q}x^2 dx = \frac{q^2}{12} \quad (8)$$

when the encoder resolution is $q$. We assume $q/t_s^2$ for the sampling period $t_s$ as the equivalent resolution of $\dot{\omega}$. See the reference [9] for the detailed derivation and assumptions.

### C. Parameter estimation based on recursive least square

Fig. 3 shows the proposed method, parameter estimation based on the RLS algorithm is performed in the RLS blocks, which robustized by the discontinuous projection, and conditional parameter updates [14], [15]. In this algorithm, when the regressor $\boldsymbol{\varphi}[k]$ at the $k$ sample satisfies the persistent excitation (PE) condition, as described below, the estimated parameter vector $\hat{\boldsymbol{\theta}}[k]$ is updated by the algorithm below using the RLS method with the $L$-sample rectangular window. In the algorithm, $\boldsymbol{P}[k]$ is the covariance matrix, and $\boldsymbol{P'}[k]$ is the intermediate matrix. $\boldsymbol{E}[k]$ is the estimation error matrix with $E_j$ as the element.

$$\hat{\boldsymbol{\theta}}[k] = \hat{\boldsymbol{\theta}}[k-1] + \mathrm{Proj}_{\hat{\boldsymbol{\theta}}}(\boldsymbol{E}[k]) \quad (9)$$

$$\begin{aligned}\boldsymbol{E}[k] =& \boldsymbol{P}[k]\varphi[k]\{y[k] - \varphi^T[k]\hat{\boldsymbol{\theta}}[k-1]\} \\ &-\boldsymbol{P}[k]\varphi[k-L]\{y[k-L] - \varphi^T[k-L]\hat{\boldsymbol{\theta}}[k-1]\}\end{aligned} \quad (10)$$

$$\boldsymbol{P}[k] = \boldsymbol{P'}[k] - \frac{\boldsymbol{P'}[k]\varphi[k-L]\varphi^T[k-L]\boldsymbol{P'}[k]}{1+\varphi^T[k-L]\boldsymbol{P'}[k]\varphi[k-L]} \quad (11)$$

$$\boldsymbol{P'}[k] = \boldsymbol{P}[k-1] + \frac{\boldsymbol{P}[k-1]\varphi[k-L]\varphi^T[k-L]\boldsymbol{P}[k-1]}{1+\varphi^T[k-L]\boldsymbol{P}[k-1]\varphi[k-L]} \quad (12)$$

$$\mathrm{Proj}_{\hat{\theta}_j}(E_j) := \begin{cases} 0 & \text{if } \hat{\theta}_j[k-1] \geq \theta_{j\max} \ \&\ E_j > 0 \\ 0 & \text{if } \hat{\theta}_j[k-1] \leq \theta_{j\min} \ \&\ E_j < 0 \\ E_j & \text{otherwise} \end{cases} \quad (13)$$

When the PE condition is not satisfied, no update is performed as $\boldsymbol{P}[k] = \boldsymbol{P}[k-1]$. Besides, the range of the estimated parameters is specified by the $\mathrm{Proj}_{\hat{\boldsymbol{\theta}}}$ function, which guarantees the minimum performance of the cutting force observer.

To design a regression model for the RLS method based on the equation of motion of the unknown parameters $J_L$, $B_L$ and $F_{CL}$ with Eq. (1), $F_{cut}$ is fundamentally unknown. Therefore, we design a regression model focusing on the frequency characteristics of the cutting force. Fig. 5 shows the results of the frequency analysis of the estimated cutting force in actual machining tests using the NVX5080 manufactured by DMG MORI CO., LTD. Note that the design parameters were applied to the cutting force observer to estimate the cutting force in the test, so it is only used as a reference value. Fig. 5 shows that the cutting force consists of a constant component and high frequency components generated when the rotating tool contacts the workpiece. According to the above characteristics, it can be assumed that $F_{cut}$ is constant in the estimated interval $L$ by filtering both sides of Eq.

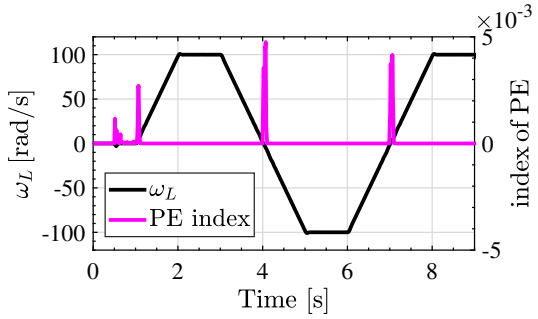


Fig. 6. Angular velocity of the system and identification difficulty of the parameter (lager is easier).

(1) using an LPF $Q_{\mathrm{RLS}}(s)$ with low bandwidth. Based on the assumption, a regression model, including the constant component of the cutting force $F_{cut}$ in the estimation interval $L$, is shown below.

$$y = \boldsymbol{\varphi}^T \boldsymbol{\theta} \tag{14}$$

where $y = Q_{\mathrm{RLS}}(s)\hat{T}_s$, $\boldsymbol{\varphi}^T = Q_{\mathrm{RLS}}(s)[\dot{\omega}_L, \omega_L, \mathrm{sgn}(\omega_L), 1]$, and $\boldsymbol{\theta} = [J_L, B_L, F_{CL}, F_{cut}^{DC}]^T$. $F_{cut}^{DC}$ corresponds to a constant component of the cutting force $F_{cut}$ and is used only for parameter estimation. This redundancy allows us to estimate model parameters under the condition which disturbance force is applied. This regression model is based on the assumption that the torsional torque $T_s$ is robust to modeling errors in previous studies [9].

Then the PE condition is considered. PE is a measure of the degree of excitation of a signal. It is guaranteed that the parameter identification converges to the actual value when the input signal is appropriately excited. In order to identify the PE condition of the state vector $\boldsymbol{\varphi}$ in proper behavior, the time variation of the minimum eigenvalue of the matrix $\boldsymbol{M}[i]$ defined in the following equation is shown as the magenta line in Fig. 6.

$$\boldsymbol{M}[i] = \frac{1}{L}\sum_{l=i-L}^{i} \boldsymbol{\varphi}[l]\boldsymbol{\varphi}[l]^T \tag{15}$$

Eq. (15) is one method for calculating index of the PE in [16], where $L$ corresponds to the estimated window length of the RLS. In Fig. 6, the PE condition is satisfied at the angular velocity reversal (i.e., change in the $\mathrm{sgn}(\omega_L)$). This behavior is considered to depend on the separability condition of $F_{CL}$ and $F_{cut}^{DC}$ in the estimated parameters. However, it is not practical to perform parameter identification only at speed reversal because of the lack of identification opportunities. Therefore, through a trial-and-error investigation, a condition in which the angular acceleration $\dot{\omega}_L$'s absolute value exceeds a threshold value is adopted as the PE condition in this paper instead of the strict PE condition. As a supplement to the above discussion, the calculation given by Eq. (15) is not suitable for online PE condition decisions because it is more advantageous to treat the amount of state as an indicator of PE condition in terms of computational complexity and tuning of identification conditions.

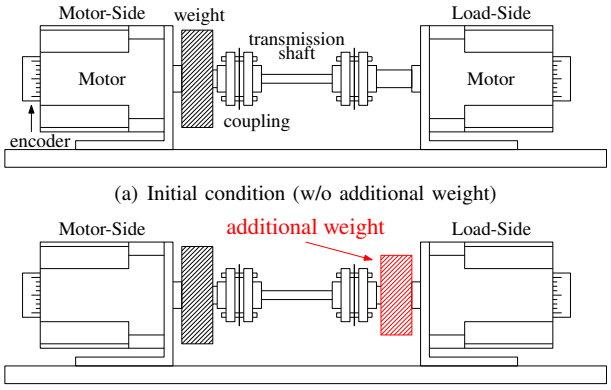


(a) Initial condition (w/o additional weight)

(b) Modified condition (w/ additional weight)

Fig. 7. Experimental setup w/ and w/o addtional weight on the load-side, simulating inertia variation during machining.

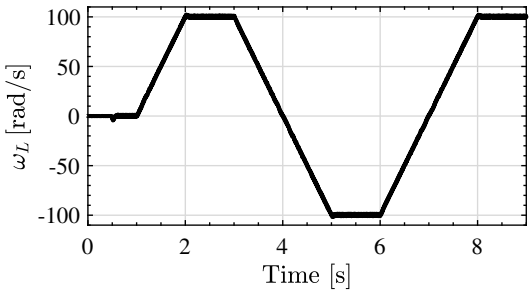


Fig. 8. Part of the trajectory of load-side angular velocity in experiment, which repeated 30 sec.

TABLE II
EXPERIMENTAL CONDITIONS.

| | | | |
|---|---|---|---|
| Sampling period | $t_s$ | 0.4 | ms |
| 20 bit encoder resolution | $q$ | $2\pi/2^{20}$ | rad |
| Estimation length of RLS | $L$ | 100 | samples |
| Cutoff frequency of $Q(s)$ | | 250 | Hz |
| Cutoff frequency of $Q_{\mathrm{RLS}}(s)$ | | 12 | Hz |

Using the load-side parameters estimated by the estimation algorithms, the cutting force observer's corresponding parameters ($J_L$, $B_L$ and $F_{CL}$ in this paper) are updated to accomplish the adaptive cutting force observer shown in Fig. 3.

## IV. EXPERIMENTAL VALIDATIONS

In order to verify the effectiveness of the proposed method, a comparison was made between the proposal (Fig. 3) and the conventional method (Fig. 4 without parameter update), which is a cutting force observer consisting of robust torsional torque estimation.

### A. Experimental conditions

In the experiments, the effectiveness of the proposed method is verified by switching the load-side parameter. First, the estimated cutting force is compared between the proposed method and the conventional method in the condition shown

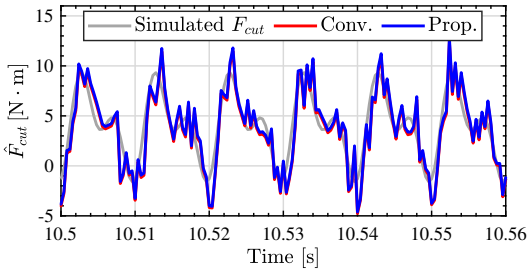


(a) w/o additional weight.

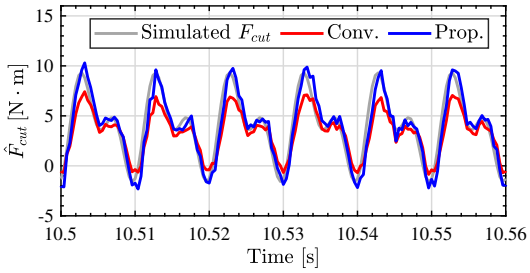


(b) w/ additional weight.

Fig. 9. $F_{cut}$ estimation comparison (w/ and w/o additional weight).

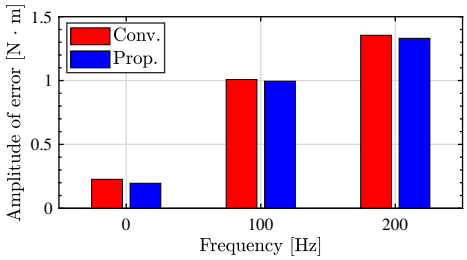


(a) w/o additional weight.

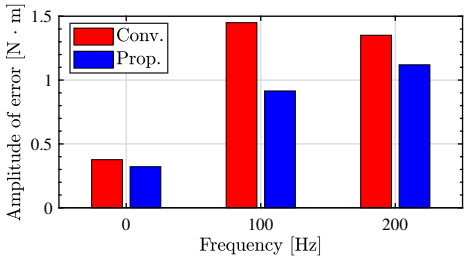


(b) w/ additional weight.

Fig. 10. $F_{cut}$ estimation error comparison in frequency domain.

TABLE III
ROOT MEAN SQUARE OF THE ESTIMATED ERRORS.

| | Prop. (adaptive) | Conv. (fixed parameters) |
|---|---|---|
| w/o additional weight | 1.950 | 1.964 |
| w/ additional weight | 1.187 | 1.532 |

in Fig. 7(a), where the observer parameters and the actual parameters are identical. Second, similar comparisons are made with changing the condition to that shown in Fig. 7(b), where a weight is attached to the load-side motor, to reproduce the inertia change. This simulates the mass change due to switch in the workpiece and other factors. Note that the design parameters of each observer were not changed through the experiments.

The parameters in Table I, which obtained in the state of Fig. 7(a) were used for observer parameter. This situation corresponds to the machine tool with nothing on the stage. The variances $\sigma_{J_M}$, $\sigma_{B_K}$, $\sigma_K$, and $\sigma_{F_{DM}}$ of the model parameters for the robust torsional torque estimation mechanism are given such that each parameter has the following errors in the $\pm 3\sigma$ interval.

$$J_M : \pm 5\,\%,\ B_M : \pm 50\,\%,\ K : \pm 30\,\%,\ F_{CM} : \pm 50\,\%$$

The parameter estimation algorithm estimates parameters within the ranges as follows [14].

$$J_L \in (0.0, \mathbb{R}),\ B_L \in (0.0, \mathbb{R}),$$
$$F_{CL} \in (0.0, \mathbb{R}),\ F_{cut}^{DC} \in \mathbb{R}$$

These ranges should designed according to feasible bounds such like machine specs. However, we approve all positive number for the estimated parameters for further discussion. Other settings, observer bandwidth, Etc., are summarized in Table II.

In the experiment, a motor on the load-side was used to apply a torque that simulates the cutting force, and the estimated cutting force was acquired. The experimental system implements a proportional–integral angular velocity control system with a multiple root pole placement at 5 Hz using the nominal plant's rigid body mode set as a controlled object. The system's angular velocity trajectory is shown in Fig. 8, assuming a reciprocating motion during machining. The angular velocity command is repeated during each experiment. The simulated cutting force is composed of a offset component of 4 N and sinusoidal vibrations with amplitudes of 4 N at frequencies of 100 Hz and 200 Hz. The simulated cutting force is based on the actual cutting force shown in Fig. 5. These experimental conditions are valid for the following reasons: the contact frequency of the tool teeth becomes dominant in heavy cutting [7], and even when an impulsive cutting force appears, the gain and phase effect due to the plant resonance can be removed by the cutting force estimation using encoders on both the motor-side and load-sides, so that higher-order harmonics can be estimated within the band of the $Q(s)$ filter.

### B. Experimental result

Fig. 9 shows The behavior of the cutting force estimations. A comparison with the initial condition is shown in Fig. 9(a), and a comparison with additional weight is shown in Fig. 9(b). There are no noticeable differences in Fig. 9(a), while significant differences are found in Fig. 9(b). To discuss these behavior, the frequency analyses of the estimation error of $\hat{F}_{cut}$ are shown in Fig. 10. It can be recognized that cutting force was well estimated for both with the proposed method (Prop.) and the conventional method (Conv.) in Fig. 10(a), where the observer parameters ware identical with

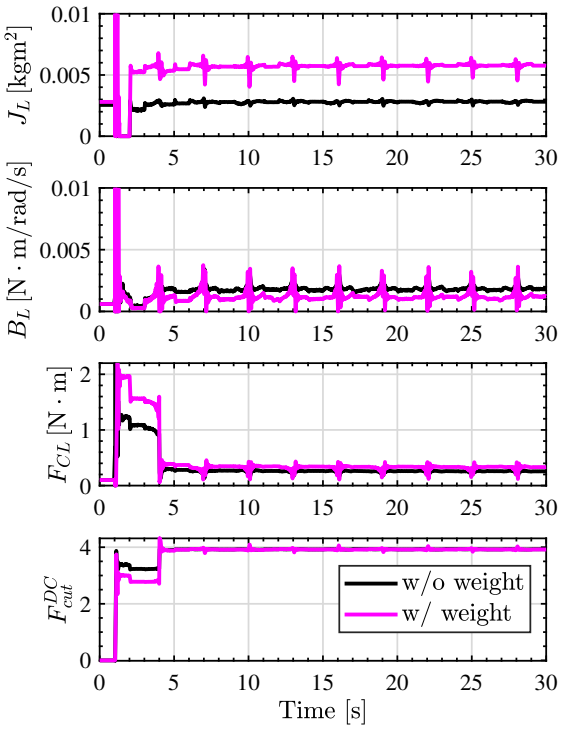


Fig. 11. Parameter estimation by RLS algorithm (black line: w/o weight, magenta line: w/ weight). $J_L$ was estimated more massive in the result with the additional wight.

actual parameters. Then, estimation error of the conventional method was significantly increased in Fig. 10(b), which was a condition with an additional weight. This thought to be caused by modeling error of $J_L$. On the other hand, the estimation accuracy of the proposal was as good as the one without the weight. Table III summarizes the root mean square (RMS) value of the estimation errors in each method in each condition. The table also shows more significant error in the conventional observer than the proposal when the observer parameters have modeling errors.

Fig. 11 shows the model parameter identification during the experiments. The black line indicates the transition of parameter identification in the initial condition, and the magenta line indicates the one after weight attached. The identified inertia $\hat{J}_L$ was more massive than the weight was attached in the comparison. The difference of $\hat{J}_L$ identification was $2.92 \times 10^{-4}\,\mathrm{kgm}^2$, which was almost equal to the actual difference. From this result, we conclude the observer's adaptation is carried out by the parameter identification and the update algorithm. However, because the strict identification condition is rarely maintained, the estimated parameters were unstable at the beginning of the experiments and estimation ripple won't stop. The proposal algorithm improved accuracy of the estimation, there is still room for further improvement.

## V. Conclusion

This paper proposed an adaptive cutting force observer which enable adaptation during the machining. The estimation accuracy of the sensorless cutting force observer can easily deteriorate by modeling error and parameter variation caused by the removal process in cutting. The proposed method solves the issue by identifying the stage parameters using the least-squares method and sequentially updating the cutting force observer using the acquired parameters. The effectiveness of the proposed method was verified by comparing it with the conventional cutting force observer in the experiments. Future research subjects include considering the validity of the identification conditions and implementation to the actual machine tools.

## References


[1] K. Javed, R. Gouriveau, X. Li, and N. Zerhouni, "Tool wear monitoring and prognostics challenges: a comparison of connectionist methods toward an adaptive ensemble model," *Journal of Intelligent Manufacturing*, vol. 29, no. 8, pp. 1873–1890, 2018.

[2] M. Nouri, B. K. Fussell, B. L. Ziniti, and E. Linder, "Real-time tool wear monitoring in milling using a cutting condition independent method," *International Journal of Machine Tools and Manufacture*, vol. 89, pp. 1–13, 2015.

[3] A. I. Azmi, "Monitoring of tool wear using measured machining forces and neuro-fuzzy modelling approaches during machining of GFRP composites," *Advances in Engineering Software*, vol. 82, pp. 53–64, 2015.

[4] H. Saraie, M. Sakahira, S. Ibaraki, A. Matsubara, Y. Kakino, and M. Fujishima, "Monitoring and Adaptive Control of Cutting Forces Based on Spindle Motor and Servo Motor Currents in Machining Centers," *Proceedings of International Conference on Leading Edge Manufacturing in 21st century : LEM21*, 2003.

[5] Y. Kakinuma and T. Kamigochi, "External sensor-less tool contact detection by cutting force observer," *Procedia CIRP*, vol. 2, no. 1, pp. 44–48, 2012.

[6] W. H. Chen, J. Yang, L. Guo, and S. Li, "Disturbance-Observer-Based Control and Related Methods - An Overview," *IEEE Transactions on Industrial Electronics*, vol. 63, no. 2, pp. 1083–1095, 2016.

[7] Y. Yamada and Y. Kakinuma, "Sensorless cutting force estimation for full-closed controlled ball-screw-driven stage," *International Journal of Advanced Manufacturing Technology*, vol. 87, no. 9-12, pp. 3337–3348, 2016.

[8] H. Kurumatani and S. Katsura, "Design of nominal parameters for robust sensorless force control based on disturbance observer," *IEEJ Journal of Industry Applications*, vol. 8, no. 2, pp. 342–351, 2019.

[9] S. Yamada and H. Fujimoto, "Minimum-variance load-side external torque estimation robust against modeling and measurement errors," *IEEJ Journal of Industry Applications*, vol. 9, no. 2, pp. 117–124, 2020.

[10] S. Yamato, A. Sugiyama, N. Suzuki, N. Irino, Y. Imabeppu, and Y. Kakinuma, "Enhancement of cutting force observer by identification of position and force-amplitude dependent model parameters," *International Journal of Advanced Manufacturing Technology*, vol. 104, pp. 3589–3605, 2019.

[11] E. Sariyildiz and K. Ohnishi, "An adaptive reaction force observer design," *IEEE/ASME Transactions on Mechatronics*, vol. 20, no. 2, pp. 750–760, 2015.

[12] M. Matsuoka, T. Murakami, and K. Ohnishi, "Vibration suppression and disturbance rejection control of a flexible link arm," *IECON Proceedings (Industrial Electronics Conference)*, vol. 2, pp. 1260–1265, 1995.

[13] J. Suzuki, T. Murakami, and K. Ohnishi, "Position and force control of flexible manipulator with position sensitive device," *International Workshop on Advanced Motion Control, AMC*, pp. 414–419, 2002.

[14] B. Yao and A. Palmer, *Indirect adaptive robust control of siso nonlinear systems in semi-strict feedback forms*. IFAC, 2002, vol. 15, no. 1.

[15] H. Fujimoto and B. Yao, "Multirate adaptive robust control for discrete-time non-minimum phase systems and application to linear motors," *IEEE/ASME Transactions on Mechatronics*, vol. 10, no. 4, pp. 371–377, 2005.

[16] K. Åström and B. Wittenmark, *Adaptive Control*, ser. Dover Books on Electrical Engineering. Dover Publications, 2008.